Complex admittance measurements in ECT for conductivity and permittivity imaging: A theoretical evaluation

Maomao Zhang[1], Yaoyuan Xu[1,2], Manuchehr Soleimani[1]

[1]Electrical tomography laboratory (ETL), Department of Electrical and Electronic Engineering, University of Bath, UK.
[2]Province-Ministry Joint Key Laboratory of Electromagnetic Field and Electrical Apparatus Reliability, Hebei University of Technology, Tianjin, China

mz215@bath.ac.uk ,m.soleimani@bath.ac.uk

ABSTRACT

A novel reconstruction method for electrical capacitance tomography is presented in this paper, where both the permittivity and the conductivity distribution of dielectric materials are considered. In order to clarify how the conductivity of background medium affects the quality of reconstructed results, detailed analysis of the relationship between the conductivity/frequency and the capacitance measurements based on complex admittance measurements are carried out. Consequently, it is found that theoretically if we can operate in higher frequency and with complex admittance measurement it may help to generate better images of both real and imaginary distribution of permittivity at the same level of conductivity. This will be especially important for the higher value of conductivity background where currently ECT fails to work. Simulations studies in this work are carried out with complex ECT electrodes are outside of an insulating pipe, and hence a truly capacitive coupled complex permittivity imaging including dielectric permittivity and electrical conductivity.

Keywords Electrical capacitance tomography, conductivity, permittivity, frequency, simulation

1. Introduction

Electrical capacitance tomography (ECT) is an imaging method that reconstructs the permittivity distribution of dielectric materials. ECT is used as part of three phase flow measurement (Huang, Plaskowski et al. 1988, Li, Yang et al. 2013, Thorn, Johansen et al. 2013), where the flow is normally of dielectric or low-conductive material. Current state of the art three phase flow imaging devices have several limitations, for example include a radiation based imaging technique (Hjertaker, Maad et al. 2011, Chaminda, Ru et al. 2014) with its radiation hazards and high cost, or a combination of electrical resistance tomography (ERT) and ECT(Wang, Huang et al. 2009) (Wang, Huang et al. 2009), with many limitation of ERT needing to be in direct contact with the medium and high cost of a dual modality ERT/ECT platform. For the conductive-background flow imaging, in (Zhang, Ma et al. 2015), Maomao et al. introduced magnetic induction tomography (MIT) as an support method to assist ECT to reconstruct the permittivity map. A dual ECT/MIT is providing promising results in case of dielectric background and promising results in conductive background, allowing separation of two dielectric phase and a conductive phase. MIT for low conductivity imaging is still under development (Ma, Hunt et al. 2015). Electrical impedance tomography (EIT) can image complex impedance (Yang, Mohammed et al. 2015) but similar to ERT requires direct contact with the conductive component of the imaging medium. In this paper we aim to investigate how much more information we can gain from ECT device assuming we can measure complex admittance in a range of frequency. ECT imaging over conductive medium is shown in (Liao and Zhou 2015), where the electrodes are in direct contact with water medium. Therefore it is essentially the same as EIT and not contactless. In (Li and Soleimani 2013), the excitation signal of higher frequency is introduced to help ECT to penetrate the

conductive water, which is also of high permittivity, and produce more information about the permittivity distribution. In (Wang, Zhang et al. 2013, Wang, Tan et al. 2014), a capacitively coupled electrical resistance tomography is used to image the conductivity distribution without contacting the conductive medium, where the permittivity is not imaged. In this study we investigate permittivity but more importantly the conductivity imaging using ECT.

A better understanding of the underlying physics is needed when it comes to conductive background ECT. This paper will attempt to answer several key questions in this regards. In this paper, we study detailed relationship between the conductivity/frequency and permittivity and the capacitance measurements based on complex admittance measurements. A complex admittance forward model can be solved and complex admittance can be then calculated. The equation below demonstrates the basic integral relation of these parameters:

$$C = -\frac{1}{U}\int(\varepsilon(x) + \frac{\sigma(x)}{i\omega})\,\nabla u(x) d\Gamma \tag{1}$$

Γ is the surface of electrode, U is the voltage on the electrode, $\varepsilon(x)$, $\sigma(x)$ and $u(x)$are the distribution of permittivity, conductivity and voltage respectively, and ω is the angular frequency of the excitation signal. Here *C* is a complex admittance between pairs of electrodes.

2. ECT model and inverse solver

The electric fields in complex ECT is governed by (Zhang, Ma et al. 2015)

$$\nabla \cdot \left(\varepsilon(x) + \frac{\sigma(x)}{i\omega}\right)\nabla u(x) = 0 \quad in\ \Omega \tag{2}$$

where Ω is the sensing region of ECT. $u(x)$ is the electric potential distribution corresponding to a set of boundary conditions given by

$$u(x) = V \qquad on\ \Gamma_{\text{excited}} \tag{3}$$

$$u(x) = 0 \qquad on\ \Gamma_{Screening}\ and\ \Gamma_{unexcited} \tag{4}$$

where V is the excitation voltage, Γ_{excited} is the surface of the excited electrode, $\Gamma_{Screening}$ is the surface of the screening and $\Gamma_{unexcited}$ is the surface of the unexcited electrodes. The electric charge on the l-th electrode is generated from the Gauss's law, as shown below.

$$Q_l = -\int_{\Gamma_l}\left[\varepsilon(x) + \frac{\sigma(x)}{i\omega}\right]\frac{\partial u(x)}{\partial n} d\Gamma \tag{5}$$

where n is the normal vector on an electrode.

Thus, the capacitance between *i*-th (which is the excitation electrode) and *j*-th (which is the detection electrode) electrodes can be calculated by

$$\mathrm{C}_{ij} = \frac{Q_j}{V_i} \tag{6}$$

Utilizing the finite element method, one can calculate the potential distribution inside the sensor and the capacitances for a given distribution of permittivity. Furthermore, one can also calculate the sensitivity maps (the change in capacitance in response to a perturbation of the permittivity distribution) according to the equation:

$$J = \frac{\partial C_{ij}}{\partial \varepsilon} = -\int_{\Omega} \nabla u_i \,.\nabla u_j dS \tag{6}$$

Since the values in equation (6) are complex, this equations can be rewritten as below

$$J_{complex} \cdot \Delta\varepsilon_{complex} = \Delta C_{complex} \tag{7}$$

$$\begin{cases} J_{complex} = J_r + iJ_i \\ \varepsilon_{complex} = \varepsilon_r + i\varepsilon_i = \varepsilon(x) + \dfrac{\sigma(x)}{i\omega} \\ C_{complex} = C_r + iC_i \end{cases}$$

Where J_r and J_i, ε_r and ε_i, C_r and C_i are the real and imaginary part of $J_{complex}$, $\varepsilon_{complex}$ and $C_{complex}$, respectively.

$$\text{Or} \qquad \begin{bmatrix} J_r & -J_i \\ J_i & J_r \end{bmatrix} \cdot \begin{bmatrix} \Delta\varepsilon_r \\ \Delta\varepsilon_i \end{bmatrix} = \begin{bmatrix} \Delta C_r \\ \Delta C_i \end{bmatrix} \tag{8}$$

Tikhnov regulation is used to calculate $\Delta\varepsilon_r$ and $\Delta\varepsilon_i$., which is explained in the equation (9).

$$\begin{bmatrix} \Delta\varepsilon_r \\ \Delta\varepsilon_i \end{bmatrix} = \left(\begin{bmatrix} J_r & -J_i \\ J_i & J_r \end{bmatrix}^T \begin{bmatrix} J_r & -J_i \\ J_i & J_r \end{bmatrix} + \alpha I \right)^{-1} \begin{bmatrix} J_r & -J_i \\ J_i & J_r \end{bmatrix}^T \begin{bmatrix} \Delta C_r \\ \Delta C_i \end{bmatrix} \tag{9}$$

Through this equation, both the real and imaginary of permittivity can be obtained.

3. Forward simulation and inverse reconstruction

3.1 Simulation of the capacitance measurements

As a time-difference method, ECT calculates the change between the capacitances of background (C_b) and sample (C_s). In table 1, the air sample is a circular region in diameter of 6cm centred at (0, 3) *cm*. The relative permittivity of the water is set as $\varepsilon_{water} = 80$, and the conductivity is increased from 0 to 1*S/m.* And frequency of the exciting voltage on the sensor is set at $f = 1.25\ MHz$. A 12 external-electrodes ECT device was considered with 66 independent measurements. An insulator layer of 0.5cm, i.e., the wall of the sensor, was considered with relative permittivity of $\varepsilon_{wall} = 3$.

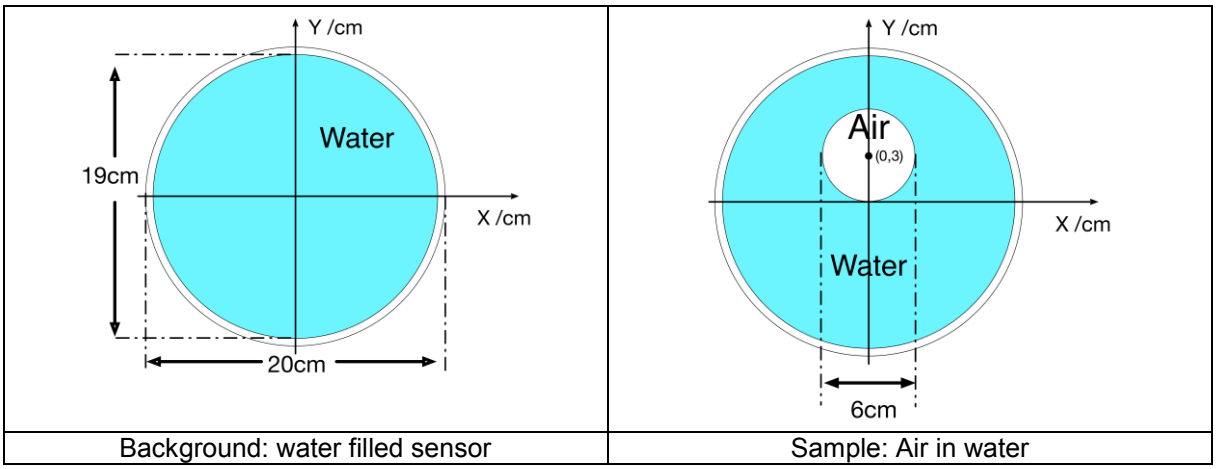

Background: water filled sensor	Sample: Air in water

Table 1. The dimensions of the ECT tank and the air sample

Since the conductivity existing in the water background within the sensor, the values of the capacitance measurements are complex values. To clearly indicate the trend of the capacitance change with increasing conductivity of background, the real and imaginary parts are plotted separated in Table 2 and 3.

	$Re(C_b)$	$Im(C_b)$
Every single inter-capacitance of any two electrodes, C_{ij}	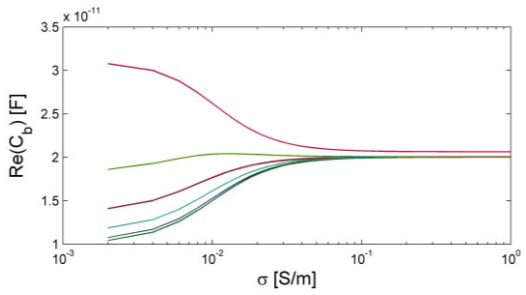	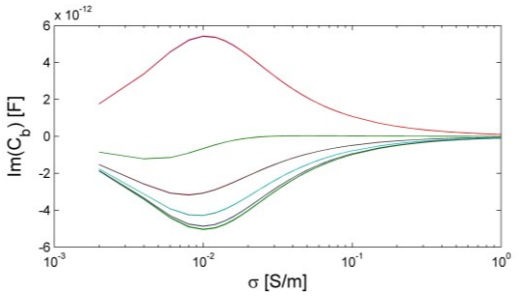
2-norm value of each set of capacitance over one conductivity	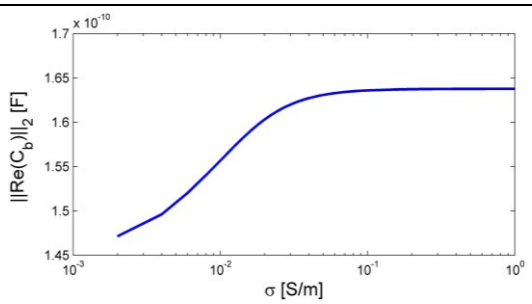	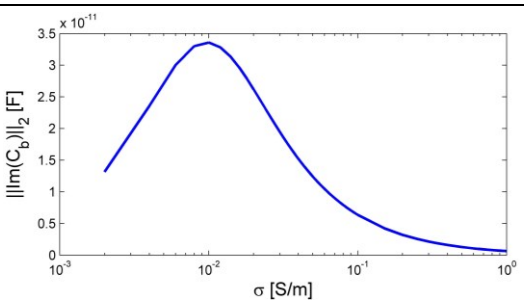

Table 2. Real and imaginary part of background capacitance, C_b

	$Re(C_s)$	$Re(C_s)$
Every single inter-capacitance of any two electrodes, C_{ij}	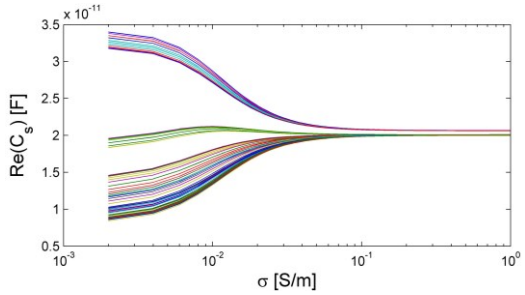	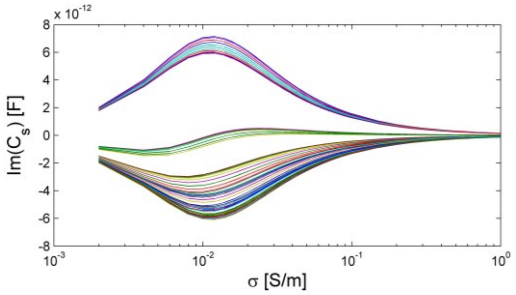
2-norm value of each set of capacitance over one conductivity	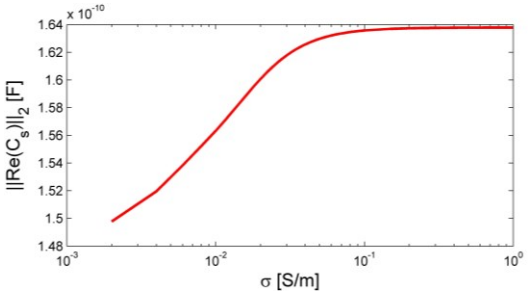	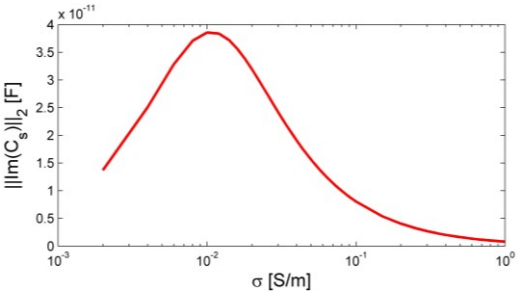

Table 3. Real and imaginary part of sample capacitance, C_s

In table 4, for the real part of the difference, the value is become relatively small when the conductivity is higher than 0.1 *S/m*. The magnitude of imaginary part reaches a peak around $\sigma = 0.016 S/m$, then declines.

	Real part of capacitance difference	Imaginary part of capacitance difference
The change in every single inter-capacitance of any two electrodes, C_{ij}	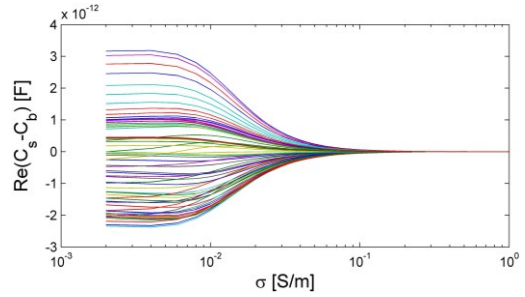	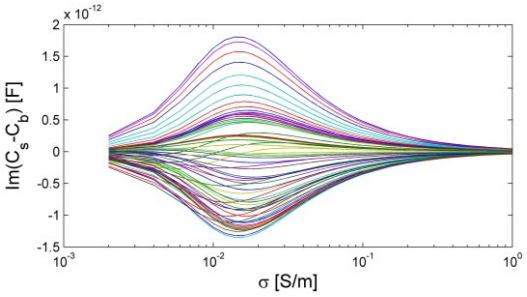
2-norm value of each set of capacitance over one conductivity	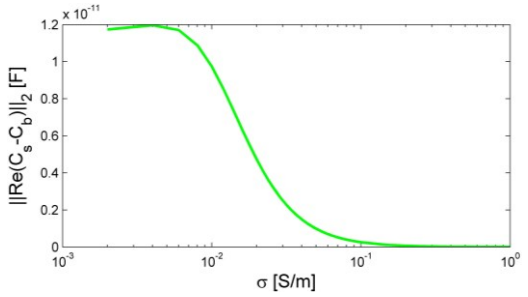	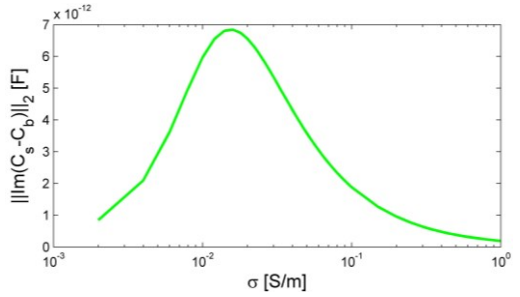

Table 4. Real and imaginary part of the capacitance difference, $C_s - C_b$

The results of tables 2-4 demonstrates that both the real and imaginary part of complex capacitance are tends to in a very small change rate as conductivity increases.

3.2 Complex permittivity reconstruction

As mentioned in equation (2), the imaginary part of complex permittivity is $\frac{\sigma}{\omega}$, Therefore, when the increasing conductivity deteriorates the imaging ability of ECT, it would be significant to adjust the frequency to recover the decaying in the measurements. In table 5, the calculated real and imaginary part of permittivity distribution is listed, where the real distribution is shown in figure 1, the dimension of the sample and sensor is the same as shown in table 1.

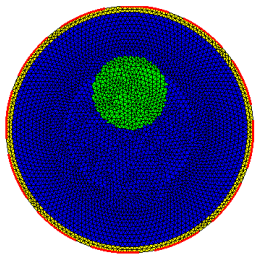

Figure 1. The real distribution model within the sensor

σ & f	$Re(\varepsilon)$	$Im(\varepsilon)$
0.1 S/m *f=1.25Mhz*	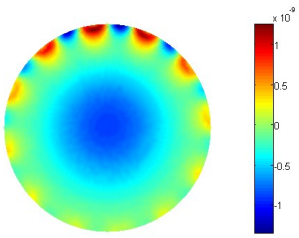	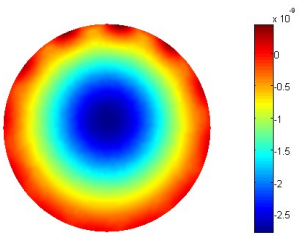
0.1 S/m *f=2.5Mhz*	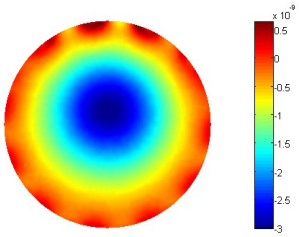	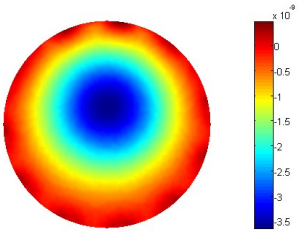
0.1 S/m *f=5Mhz*	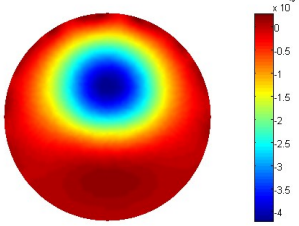	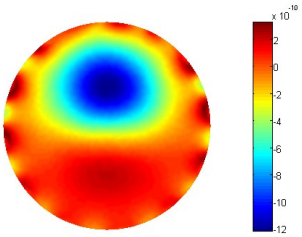

Table 5. The ECT images of an air sample standing in water of conductivity of 0.1S/m at different frequency

4. Conclusions

ECT is used as method to imaging permittivity distribution for a long time. In this paper, both real and imaginary parts of the complex permittivity are investigated through simulation modelling. Extensive number of simulation studies was carried out and only a small number of selected results are shown here. The imaginary part provides similar level of information of the real part, which stands for the real permittivity distribution. Since both the conductivity and frequency affects the measurement of the complex capacitance, applying higher frequency to ECT measurement may help to generate better images of both real and imaginary distribution of permittivity at the same level of conductivity. This is important as for the higher value of conductivity backgrounds ECT fails to work. More experimental work on different frequencies will be carried out based on an impedance analyser, instead of a purely capacitance measurement unit. Therefore, the feasibility of the multi-frequency complex admittance ECT method will be tested.

REFERENCES

Chaminda, P., Y. Ru, V. Sondre, C. M. Morten and M. Saba (2014). "Electrical capacitance tomography (ECT) and gamma radiation meter for comparison with and validation and tuning of computational fluid dynamics (CFD) modeling of multiphase flow." Measurement Science and Technology **25**(7): 075404.

Hjertaker, B. T., R. Maad and G. A. Johansen (2011). "Dual-mode capacitance and gamma-ray tomography using the Landweber reconstruction algorithm." Measurement Science and Technology **22**(10): 104002.

Huang, S., A. Plaskowski, C. Xie and M. Beck (1988). "Capacitance-based tomographic flow imaging system." Electronics letters **24**(7): 418-419.

Li, Y. and M. Soleimani (2013). "Imaging conductive materials with high frequency electrical capacitance tomography." Measurement **46**(9): 3355-3361.

Li, Y., W. Yang, C.-g. Xie, S. Huang, Z. Wu, D. Tsamakis and C. Lenn (2013). "Gas/oil/water flow measurement by electrical capacitance tomography." Measurement Science & Technology **24**(7).

Liao, A. and Q. Zhou (2015). "Application of ECT and relative change ratio of capacitances in probing anomalous objects in water." Flow Measurement and Instrumentation **45**(0): 7-17.

Ma, L., A. Hunt and M. Soleimani (2015). "Experimental evaluation of conductive flow imaging using magnetic induction tomography." International Journal of Multiphase Flow **72**(0): 198-209.

Thorn, R., G. A. Johansen and B. T. Hjertaker (2013). "Three-phase flow measurement in the petroleum industry." Measurement Science and Technology **24**(1): 012003.

Wang, B., Z. Huang and H. Li (2009). Design of high-speed ECT and ERT system. Journal of Physics: Conference Series, IOP Publishing.

Wang, B., W. Tan, Z. Huang, H. Ji and H. Li (2014). "Image reconstruction algorithm for capacitively coupled electrical resistance tomography." Flow Measurement and Instrumentation **40**(0): 216-222.

Wang, B., W. Zhang, Z. Huang, H. Ji and H. Li (2013). "Modeling and optimal design of sensor for capacitively coupled electrical resistance tomography system." Flow Measurement and Instrumentation **31**(0): 3-9.

Yang, C. L., A. Mohammed, Y. Mohamadou, T. I. Oh and M. Soleimani (2015). "Complex conductivity reconstruction in multiple frequency electrical impedance tomography for fabric-based pressure sensor." Sensor Review **35**(1): 85-97.

Zhang, M., L. Ma and M. Soleimani (2015). "Dual modality ECT–MIT multi-phase flow imaging." Flow Measurement and Instrumentation.